

RED CELLS, IRON, AND ERYTHROPOIESIS

CD63 is regulated by iron via the IRE-IRP system and is important for ferritin secretion by extracellular vesicles

Izumi Yanatori,¹ Des R. Richardson,^{1,2,*} Herschel S. Dhekne,³ Shinya Toyokuni,^{1,4,*} and Fumio Kishi⁵

¹Department of Pathology and Biological Responses, Nagoya University Graduate School of Medicine, Nagoya, Japan; ²Centre for Cancer Cell Biology and Drug Discovery, Griffith Institute for Drug Discovery, Griffith University, Nathan, Brisbane, QLD, Australia; ³Department of Biochemistry, Stanford University School of Medicine, Stanford, CA; ⁴Center for Low-Temperature Plasma Sciences, Nagoya University, Nagoya, Japan; and ⁵Kenjinkai Healthcare Corporation, Yamaguchi, Japan

KEY POINTS

- CD63 is involved in EV secretion from cells and is shown herein to be regulated by iron via the IRE-IRP system.
- Iron-loading increased secretion of CD63⁺ EVs containing iron-loaded ferritin.

Extracellular vesicles (EVs) transfer functional molecules between cells. CD63 is a widely recognized EV marker that contributes to EV secretion from cells. However, the regulation of its expression remains largely unknown. Ferritin is a cellular iron storage protein that can also be secreted by the exosome pathway, and serum ferritin levels classically reflect body iron stores. Iron metabolism-associated proteins such as ferritin are intricately regulated by cellular iron levels via the iron responsive element-iron regulatory protein (IRE-IRP) system. Herein, we present a novel mechanism demonstrating that the expression of the EV-associated protein CD63 is under the regulation of the IRE-IRP system. We discovered a canonical IRE in the 5' untranslated region of CD63 messenger RNA that is responsible for regulating its expression in response to increased iron. Cellular iron loading caused a marked increase in CD63 expression and the secretion of CD63⁺ EVs

from cells, which were shown to contain ferritin-H and ferritin-L. Our results demonstrate that under iron loading, intracellular ferritin is transferred via nuclear receptor coactivator 4 (NCOA4) to CD63⁺ EVs that are then secreted. Such iron-regulated secretion of the major iron storage protein ferritin via CD63⁺ EVs, is significant for understanding the local cell-to-cell exchange of ferritin and iron.

Introduction

Extracellular vesicles (EVs) are released by cells and are found in most biological fluids.¹ EVs can be produced by fusion of endosomal multivesicular bodies within the plasma membrane, which releases intraluminal vesicles in the form of exosomes.² CD63 and CD81 are tetraspanin superfamily members and are highly expressed in EVs.³ CD63 is localized to intraluminal vesicles of late endosomes and multivesicular bodies and is enriched in EVs.^{4,5} Intriguingly, CD63 contributes to EV secretion.⁶ CD63 has also been suggested to play a variety of roles in, for instance, platelet activation and cell signaling,⁷ as well as after viral infection and may have a role in increasing EV biogenesis.⁸ Ferritin is the major intracellular iron storage protein^{9,10} and is also found extracellularly in EVs.^{11,12}

However, mammalian ferritin lacks the signal peptide for endoplasmic reticulum-Golgi secretion in spite of its presence in serum.¹¹ A range of cell types secrete ferritin, including hepatocytes,¹³ hepatoma cells,¹⁴⁻¹⁶ endothelial cells,¹⁷ erythroid leukemia cells,¹⁸ macrophages,¹⁹⁻²² fibroblasts,²³ neuroblastoma cells,^{24,25} oligodendrocytes,²⁶ and astrocytes.²⁷ Ferritin secretion occurs by poorly defined processes with iron-rich ferritin being released via the multivesicular body-EV (exosome) pathway.¹²

Serum ferritin reflects body iron stores and is a hematologic index used to monitor iron-associated diseases.²⁸

The mechanism for regulating ferritin secretion by cellular iron remains unknown.¹² Considering the regulation of intracellular ferritin by iron, when iron levels increase, ferritin is rapidly induced by halting posttranscriptional inhibition through the iron-responsive element-iron-regulatory protein (IRE-IRP) system.^{29,30} This avoids free unbound iron, which is toxic.³¹ The iron regulatory proteins IRP1 and IRP2 bind to IREs (Figure 1A-B) in the 3' or 5' untranslated regions (UTRs) of messenger RNAs (mRNAs).³² The IREs form hairpin structures composed of a stem and a loop, with the canonical apical IRE loop sequence consisting of 6 nucleotides (CAG(U/A)GN) (Figure 1A-B).³³⁻³⁵

Herein, we demonstrate for the first time that CD63 plays a role in EV secretion⁶ and is posttranscriptionally regulated by iron via the IRE-IRP system, and excess iron induces CD63 expression. Under iron loading, intracellular ferritin is transferred via nuclear receptor coactivator 4 (NCOA4)/ferritin vesicles to CD63⁺ EVs that are secreted. Such iron-regulated secretion of ferritin via CD63⁺ EVs helps us understand how iron metabolism is regulated at the local cell-to-cell level.

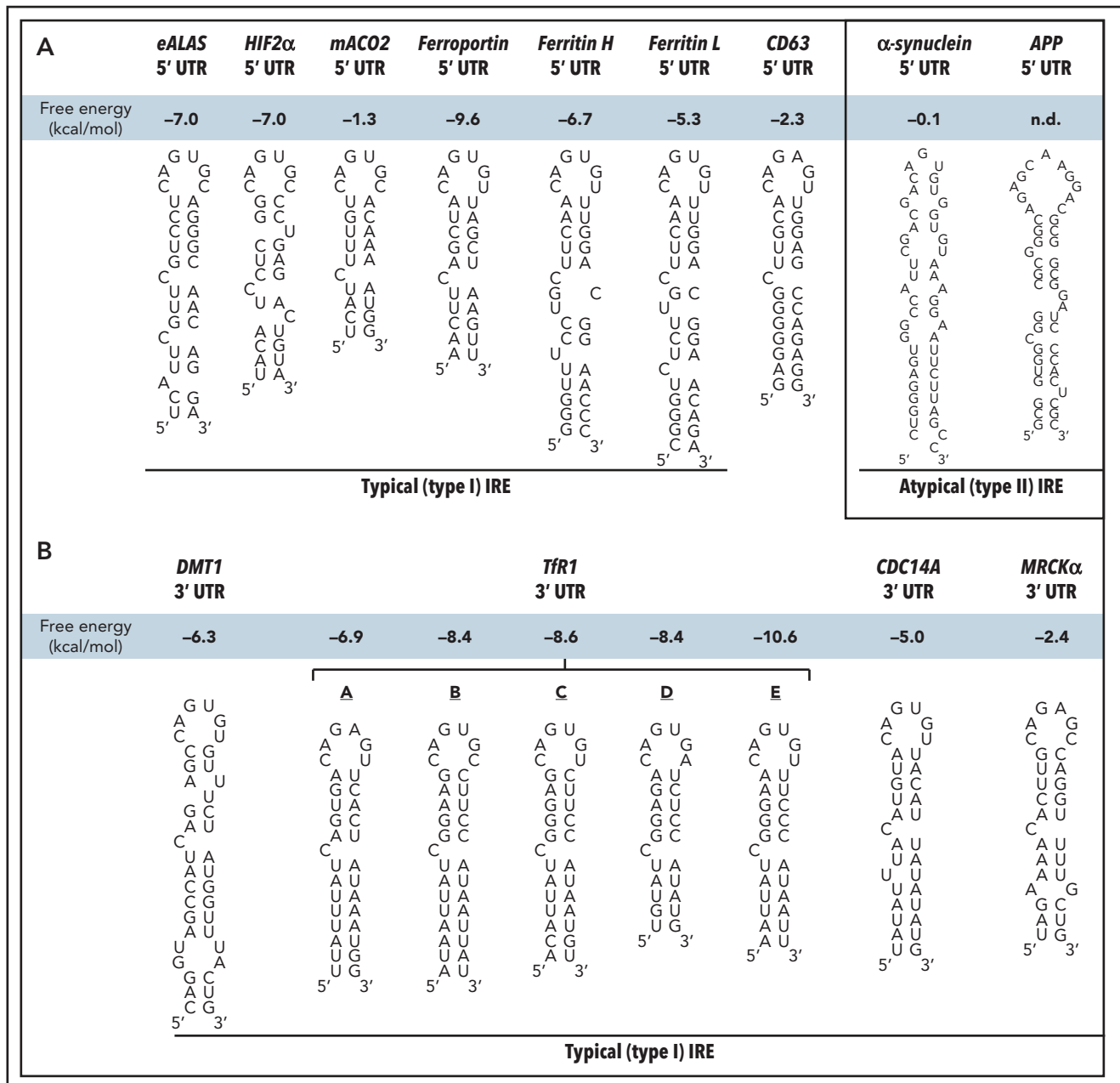


Figure 1. Schematic illustration of the sequences/structures of IREs. (A) Schematic illustration of the structures of typical (type I) IRE stem loops in the 5' UTRs of the mRNAs of erythroid delta aminolevulinic acid synthase (*eALAS*), hypoxia inducible factor-2 α (*HIF-2 α*), mitochondrial aconitase 2 (*mACO2*), ferroportin, *FTH*, *FTL*, and *CD63* relative to the atypical (type II) IREs in the 5' UTR of α -synuclein and amyloid precursor protein (*APP*). (B) Schematic illustration of the structures of typical (type I) IRE stem loops in the 3' UTR regions of the mRNAs of divalent metal ion transporter 1 (*DMT1*), transferrin receptor 1 (*TfR1*; 5 *TfR1* IREs are denoted: A-E), cell division cycle 14A (*CDC14A*) and myotonic dystrophy kinase-related CDC42-binding kinase- α (*MRCK α*). n.d., not determined.

Methods

All protocols are described in detail in the supplemental Methods available on the *Blood* Web site.

Collection of EVs from cellular supernatants

IMR90SV cells were incubated with 0, 5, or 20 μ g/mL ferric ammonium citrate (FAC) for 48 hours at 37°C supplemented with 0.5% fetal bovine serum (FBS) depleted of bovine EVs. EVs were collected from cellular supernatants by a well-characterized protocol.³⁶

RNA pulldown

The IRE region of *CD63* mRNA (NM_001257389.2 on National Center for Biotechnology Information) was analyzed by using the Search for Iron-Responsive Elements (SIREs) Web Server 2.0 (<http://ccbgi.imppc.org/sires/>).³⁷ The predicted IRE of *CD63* 5' UTR RNA (5'-GAGGGGGCUUGCACAGAGUUGGAGCCA-GAGG-3') was synthesized by Eurofins Scientific. The RNA 3' end was biotinylated using a Pierce RNA 3' End Biotinylation Kit. Biotinylated RNA was mixed with precleared total protein extracts from IMR90SV cells (recombinant glutathione S-transferase [GST]-IRP1, or GST-IRP2) and magnetic streptavidin

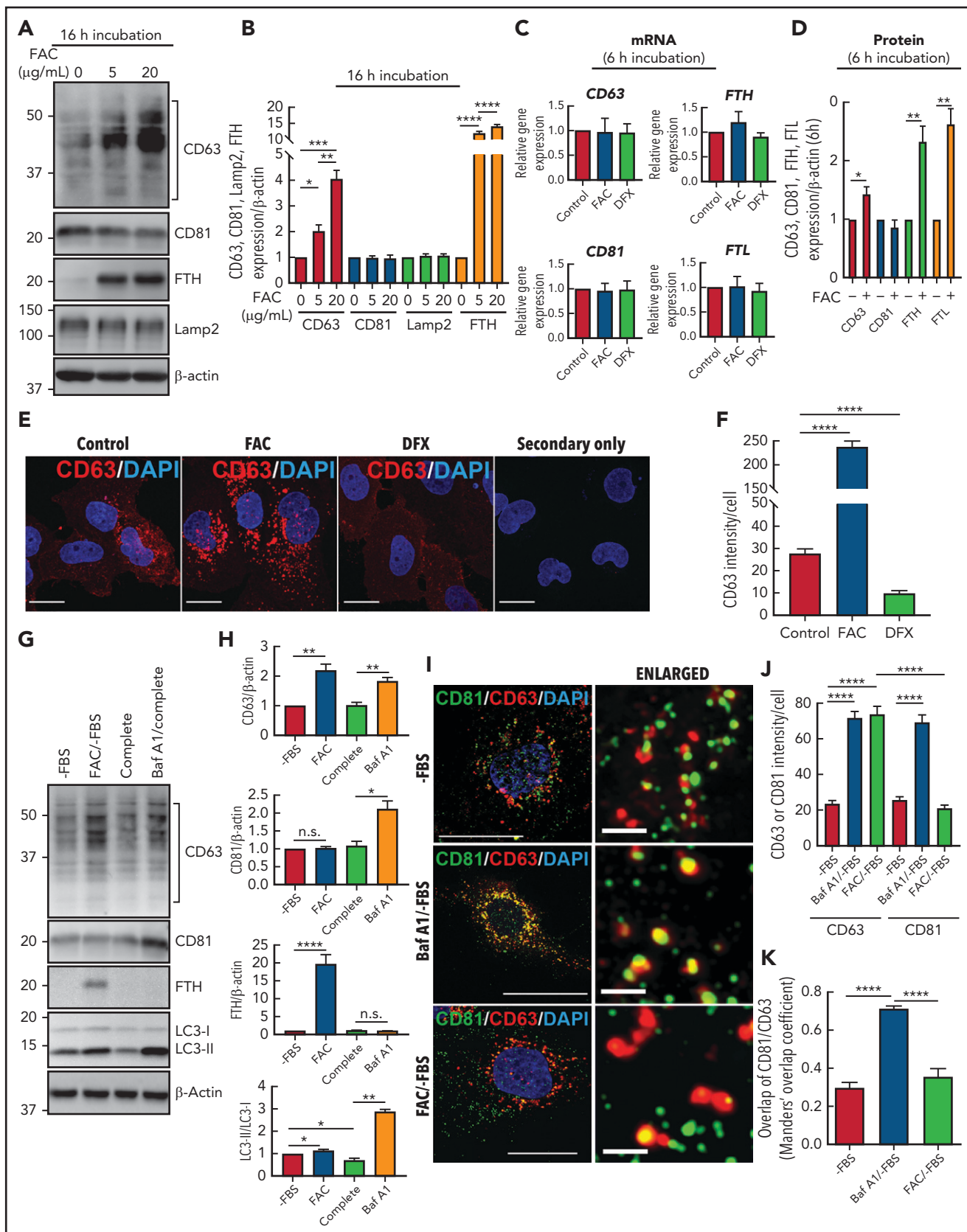


Figure 2. CD63 expression is increased by cellular iron loading and decreased by iron depletion. (A) IMR90SV cells were incubated for 16 hours at 37°C with either control medium or medium containing FAC (5 or 20 µg/mL) without FBS (–FBS). Cells were then lysed in lysis buffer, and 20 µg of protein from each sample was analyzed with anti-CD63, anti-CD81, anti-FTH, anti-Lamp2, and anti- β -actin antibodies using immunoblotting. (B) Quantification of CD63, CD81, and Lamp2 intensity from panel A. (C) IMR90SV cells were incubated with 10 µg/mL FAC or 50 µM DFX for 6 hours at 37°C in media (–FBS). The relative mRNA levels of CD63, CD81, FTH, and

R280 beads were then added to the mixture. Samples were analyzed by immunoblotting.

Electrophoretic mobility shift assay (EMSA)

The reactions included 62.5 nM biotinylated RNA and 0.5 μ g purified GST-IRP1 or GST-IRP2 with unlabeled RNA competitors. The binding reactions for RNAs and GST-IRP1 or GST-IRP2 were electrophoresed and transferred to a nylon membrane. The biotinylated RNA was detected with streptavidin-horseradish peroxidase (#P0397; Dako, Santa Clara, CA).

Results

CD63 expression is upregulated by iron loading

The EV pathway is involved in ferritin secretion,¹² although its regulation by iron levels has not been investigated. Both CD63 and CD81 are key to EV production³⁸ and are important to examine in terms of their regulation by iron. Because ferritin is secreted by a range of cells,¹³⁻²⁷ initial studies used fibroblasts, which secrete ferritin in exosomes.²³

In these experiments, human IMR90SV fibroblasts were incubated for 16 hours at 37°C in the absence of FBS (hereafter –FBS) with FAC (0, 5, or 20 μ g/mL), which increases functional iron pools.^{14,15,39} CD63 and CD81 expression in cell lysates was then examined by immunoblotting (Figure 2A-B). The levels of CD63 showed significant ($P < .001$ to $P < .05$) upregulation upon incubation of cells with increasing FAC concentration compared with the control (Figure 2A-B). The immunoblots revealed that CD63 expression consisted of a ladder banding pattern at ~30 to 60 kDa, with a major band being identified at ~40 kDa (Figure 2A). These CD63 bands are the result of differential glycosylation^{40,41} and were included in the densitometric analysis. Similar to CD63, ferritin-H (FTH) chain was also significantly ($P < .0001$) upregulated by FAC compared with the control.^{10,14} In contrast to CD63 and FTH, no significant change in CD81 or the lysosomal marker Lamp2 was observed after incubation with FAC (Figure 2A-B).

After a 6-hour incubation with FAC (10 μ g/mL) or deferiasirox (DFX; 50 μ M), CD63, CD81, FTH, or FTL mRNA levels were not changed (Figure 2C), whereas the protein expression of CD63, FTH, and FTL was significantly ($P < .01$ to $P < .05$) enhanced by a 6-hour incubation with FAC (10 μ g/mL; Figure 2D). These data suggest posttranscriptional regulation, as previously observed for ferritin.^{42,43}

In agreement with the immunoblotting shown in Figure 2A-B, immunostaining of CD63 in IMR90SV cells treated with FAC under the same conditions (16 hours at 37°C [–FBS]) revealed a significant ($P < .0001$) eightfold increase in CD63 compared with the respective control (Figure 2E-F). In contrast, iron depletion induced by incubation (16 hours [–FBS]) with the well-characterized iron chelator DFX (5 μ M)^{44,45} significantly ($P < .0001$) decreased CD63 by >50% compared with the control (Figure 2E-F). Comparable results demonstrating iron-regulated expression of CD63, but not CD81, were also obtained after incubating HeLa and HepG2 cells with FAC or DFX for 16 hours at 37°C (supplemental Figure 1A-H). Collectively, CD63 was regulated by iron in multiple cell types.

Iron-induced CD63 expression occurs by a different mechanism than CD63 induction by autophagic inhibition

Inhibition of autophagy after bafilomycin A1 (Baf A1) results in inhibition of autophagosome-lysosome fusion and increases CD63 and CD81.⁴⁶ Autophagy is a catabolic process, and in terms of iron metabolism, iron loading (an anabolic effect) may inhibit autophagy. So, we considered whether the effect of iron (as FAC) at increasing CD63 expression (Figure 2A-F) was a result of autophagic inhibition. Autophagy is often modulated by 2 methods: (1) FBS depletion that can initiate autophagy, and (2) the late-stage inhibitor of autophagy, Baf A1, inhibits autophagosome-lysosome fusion.^{47,48} Thus, IMR90SV cells were incubated for 12 hours at 37°C with medium (–FBS) (the control), medium containing FAC (10 μ g/mL) (–FBS), complete media (ie, with FBS), or Baf A1 (2 nM) in complete media (Figure 2G-H). The addition of FAC to media (–FBS) led to the same results as those shown in Figure 2A-B, with a significant ($P < .0001$ to $P < .01$) increase in CD63 and FTH expression, whereas there was no significant ($P > .05$) change in CD81 expression (Figure 2G-H).

To examine alterations in autophagy, expression of microtubule-associated protein 1 light chain 3 (LC3) was assessed.⁴⁹ Autophagic initiation is examined by assessing conversion of LC3-I (cytosolic form) to LC3-II (autophagosome membrane-bound form), with LC3-II being a classical autophagosome marker that correlates with autophagosome number.⁴⁷ During autophagy, proteins are targeted to autophagosomes, which fuse with lysosomes to generate autolysosomes.⁵⁰ Supplementation of media (–FBS) with FAC resulted in a slight increase ($P < .05$) in LC3-II compared with the control (–FBS) (Figure 2G-H). This is consistent with mild inhibition of autophagy by iron loading.

Figure 2 (continued) FTL were calculated using the 2^{-ΔΔC_q} method and normalized to glyceraldehyde-3-phosphate dehydrogenase (GAPDH). (D) IMR90SV cells were incubated with 10 μ g/mL FAC for 6 hours at 37°C in media (–FBS). Cells were then lysed in lysis buffer, and 20 μ g of each sample was analyzed with anti-CD63, anti-CD81, anti-FTH, anti-FTL, and anti- β -actin antibodies using immunoblotting. (E) IMR90SV cells were incubated with either control medium (–FBS) or medium containing 10 μ g/mL FAC or 5 μ M DFX for 16 hours at 37°C. Cells were fixed and stained with anti-CD63 antibodies (red) and 4',6-diamidino-2-phenylindole (DAPI; blue). As a negative control, IMR90SV cells were incubated with 10 μ g/mL FAC for 16 hours at 37°C and were treated with secondary antibody without primary antibody. Scale bar, 10 μ m. (F) Quantification of CD63 intensity per cell was performed with >60 cells examined per condition from 3 experiments. (G) IMR90SV cells were incubated with medium (–FBS) (control), with 10 μ g/mL FAC (–FBS), 10% FBS complete medium (complete), or complete medium containing 2 nM bafilomycin A1 (Baf A1/complete) for 12 hours at 37°C. Then, 20 μ g of protein per sample was examined using immunoblotting analysis. (H) Quantification of CD63, CD81, FTH, and LC3-II intensity of entities in panel G. (I) Confocal immunofluorescence microscopy of IMR90SV cells. Cells were cultured with medium (–FBS), medium containing 2 nM Baf A1 (–FBS), or medium containing 10 μ g/mL FAC (–FBS) for 12 hours at 37°C. Cells were then fixed and stained with anti-CD81 (green), anti-CD63 (red), and DAPI (blue). Thin scale bar, 10 μ m; thick scale bar (for enlarged photos), 2.5 μ m. (J) Quantification of CD63 or CD81 intensity per cell. (K) Calculation of the Manders' overlap coefficient assessing CD63 and CD81 overlap. For panels J and K, data are from examining >60 cells per condition over 3 experiments. Quantification of CD81 and CD63 colocalization was determined via the Manders' overlap coefficient. All results are mean \pm standard error of the mean (SEM) from 3 representative experiments. Significance was determined using the Student t test. * $P < .05$; ** $P < .01$; *** $P < .001$; **** $P < .0001$. n.s., not significant.

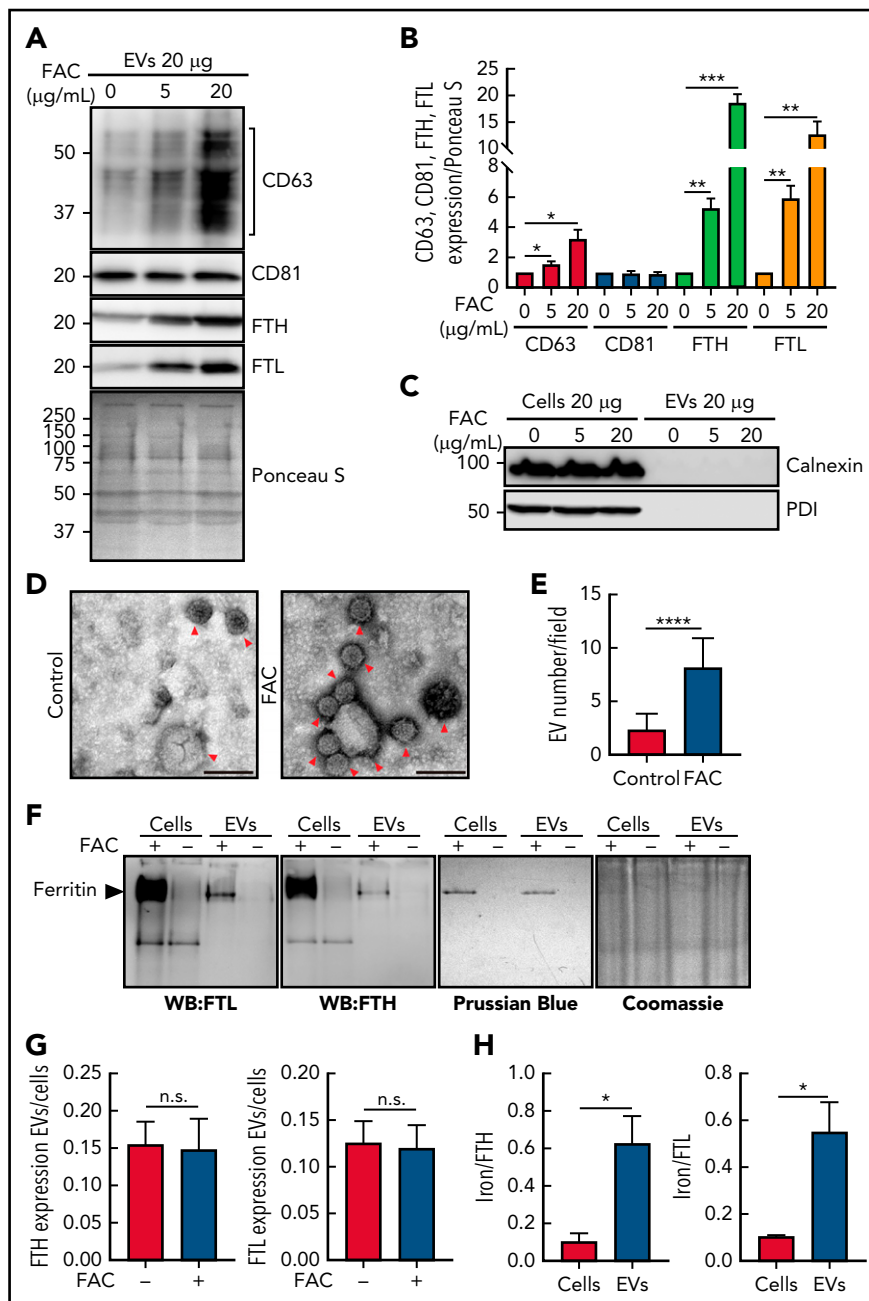


Figure 3. Increasing cellular iron after incubation with FAC upregulates CD63, FTH, and FTL expression in isolated EVs with the ferritin in EVs containing iron.

(A) IMR90SV cells were incubated with medium containing 0 (control), 5, or 20 µg/mL FAC for 48 hours at 37°C. (A) EVs and (C) EVs or cells were prepared in lysis buffer, the protein concentration was measured by a bicinchoninic acid (BCA) protein assay, and 20 µg of protein from each sample was analyzed using anti-CD63, anti-CD81, anti-FTH, anti-FTL, anti-calnexin, and anti-protein disulphide-isomerase (PDI) antibodies. (B) Quantification of CD63, CD81, FTH and FTL shown in panel A using Fiji software. Expression was normalized by Ponceau S staining as in panel A. (D) Representative transmission electron microscope images of isolated EVs from IMR90SV cells with negative staining by uranyl acetate. Red arrowheads show EVs. Scale bar, 100 nm. (E) Quantification of EV number per field in panel D. Thirty transmission electron micrograph fields over 3 experiments (>90 fields) at an original magnification of 20000× were randomly chosen, and EVs were counted by a blinded investigator (up to 500 to 1000 vesicles were counted per experiment). (F) IMR90SV cells incubated with FAC (10 µg/mL) for 48 hours at 37°C express high levels of FTH and FTL in cells and EVs, as demonstrated by native polyacrylamide gel electrophoresis (PAGE) and immunoblotting (20 µg protein per well; western blotting (WB), left-hand membranes). The same samples were simultaneously run under native PAGE conditions and stained with Prussian blue (60 µg of protein/lane) to identify Fe³⁺. Coomassie blue staining of the gel was used to verify equal protein loading; full-lane densitometry of staining showed no difference with or without FAC treatment. (G) Ratios of FTH and FTL expression in EVs and cells after densitometric analysis of the results in panel F. (H) Iron:FTH or iron:FTL ratios in cells or EVs after densitometric analysis of the results in panel F. Results are mean ± SEM (3 experiments). Significance was determined using the Student t test. **P* < .05; ***P* < .01; ****P* < .001; *****P* < .0001.

Inhibition of autophagosome-lysosomal fusion by incubation with Baf A1 in complete media increased CD63 (*P* < .01) and CD81 (*P* < .05) compared with the complete media control, as demonstrated previously.⁴⁶ In contrast, Baf A1 did not alter the

low FTH expression compared with the complete medium control. The addition of Baf A1 also resulted in an increase in LC3-II (*P* < .01) compared with the control, which is expected based on the failure of autophagosomes to fuse with lysosomes,

Table 1. Conserved sequences of CD63 IREs in various species

Conserved CD63 IREs species	Common name	Predicted sequences	Free energy (kcal/mol)	IRE motif classification
<i>Homo sapiens</i>	Human	GAGGGGGCUUGC ACAGAGU UGGAGCCAGAGG	-2.3	Typical
<i>Pan paniscus</i>	Bonobo; pygmy chimpanzee	GAGGGGGCTTGC ACAGAGT TGGAGCCAGAGG	-2.3	Typical
<i>Pan troglodytes</i>	Chimpanzee	GAGGGGGCUUGC ACAGAGU UGGAGCCAGAGG	-2.3	Typical
<i>Gorilla gorilla</i>	Western gorilla	GACGGGGCUUGC ACAGAGU UGGAGCCAGAGG	-2.3	Typical
<i>Theropithecus gelada</i>	Gelada; gelada baboon	UUUCCGGGU GGGAGG GGCCGGGAAUCG	-4.3	SELEX
<i>Bos taurus</i>	Cattle	CCCCCUCAUCC GGGAGG GGGGUAAUAC	-3.4	SELEX
<i>Sus scrofa</i>	Pig	CCUGAGCCGCG GGGAGU GCAGCGCACAGC	-8.4	SELEX
<i>Peromyscus leucopus</i>	White-footed mouse	CCUGAGCCGCG GGGAGU GCAGCGCACAGC	-8.4	SELEX
<i>Ovis aries</i>	Sheep	CAGCCCCUCAUC CAGGGG AGUGGGUAAUA	-2.3	SELEX
<i>Capra hircus</i>	Goat	CAGCCCCUCAUC CAGGGG AGUGGGUAAUA	-2.3	SELEX
<i>Camelus dromedarius</i>	Arabian camel	CCUGAGCCG CAGCGGGAGAG CAGCGCACAGC	-8.8	SELEX
<i>Mesocricetus auratus</i>	Golden hamster	CGGCGCCGGUUC CAGUGAGG CCCCGGGAA	-6.4	SELEX
<i>Physeter catodon</i>	Sperm whale	CCUGAGCCGCG GGGAGAG CAGCGCACAGC	-9.2	SELEX

Characters in bold indicate loop structure in the CD63 IRE; characters not shown in bold type indicate the predicted stem sequences. Typical (type I) canonical IRE motifs: 5'-CAG(U/A)GN-3'. The systematic evolution of ligands by exponential enrichment motif (SELEX) has been demonstrated to bind IRP1 and/or IRP2 in vitro.^{32,37}

which prevents the degradation of LC3-II (Figure 2G-H). Treatment with Baf A1 and its effect on LC3-II acted as a positive control for its activity. Collectively, these studies (Figure 2G-H) demonstrated that upregulation of CD63 and CD81 via the inhibition of autophagy by Baf A1 was distinct from the effect of FAC, which upregulated ferritin and CD63 expression but not CD81 expression.

Further studies analyzed the subcellular localization of CD81 and CD63 by using confocal microscopy. In these experiments, IMR90SV cells were incubated for 12 hours with control medium (-FBS) (control) or this medium containing either Baf A1 or FAC. Under control conditions (-FBS), CD63 (red) and CD81 (green) demonstrated weak colocalization, whereas incubation with Baf A1 (-FBS) induced a significant ($P < .0001$) increase in colocalization between CD63 and CD81 (yellow; Figure 2I-K). Baf A1 prevents fusion of lysosomes and autophagosomes and results in autophagosome accumulation,^{47,48} which suggests that the colocalization of CD63 and CD81 is occurring in autophagosomes. In contrast, when cells were incubated with FAC (-FBS), there was no significant ($P > .05$) difference in colocalization between CD63 and CD81 compared with the control (-FBS) (Figure 2I-K). In agreement with the immunoblotting (Figure 2A-B,G-H), incubation with FAC (-FBS) increased CD63 expression but had no effect on CD81 expression (Figure 2I-K).

To assess whether other metals induce CD63 expression, its mRNA and protein levels were measured after loading IMR90SV fibroblasts with ZnSO₄ (40 μM; supplemental Figure 2A-E). After loading cells with Zn(II), levels of zinc were significantly ($P < .0001$) increased (supplemental Figure 2A-B), whereas neither CD63, CD81, FTH, and FTL mRNA levels (supplemental Figure

2C) nor their protein levels (supplemental Figure 2D-E) were significantly altered compared with the control.

In summary, Figure 2 and supplemental Figure 2 show that the major EV components CD63 and CD81 are upregulated by Baf A1, whereas only CD63 is upregulated by cellular iron loading with FAC.

Iron induces secretion of CD63 and ferritin in EVs

Next, we analyzed loading cells with iron using FAC and examining CD63, CD81, and FTH and FTL expression in secreted EVs (Figure 3). In these studies, IMR90SV fibroblasts (Figure 3) and the human THP1 monocytic cell line (supplemental Figure 3) were cultured for 48 hours at 37°C with FAC at 0, 5, or 20 μg/mL. This medium contained 0.5% FBS that had already been depleted of bovine EVs,⁵¹ and this low FBS level was used to maintain cellular viability. After the 48-hour incubation of cells with and without FAC, the culture supernatant was decanted and examined for CD63, CD81, FTH, and FTL (Figure 3A-B; supplemental Figure 3).

The expression of CD63 in EVs obtained from supernatants from IMR90SV fibroblasts demonstrated a pronounced and significant ($P < .05$) increase upon incubation of cells with increasing FAC (Figure 3A-B). In contrast, there was no change in CD81 expression in EVs upon iron loading (Figure 3A-B), which was in agreement with the absence of any alteration in cellular CD81 after incubation with FAC (Figure 2A-B). Of note, there was a marked and significant ($P < .001$ to $P < .0001$) increase in the expression of FTH and FTL in EVs from IMR90SV fibroblasts as a function of FAC concentration (Figure 3A-B). Results analogous to those found in IMR90SV cells (Figure 3A-B) were also

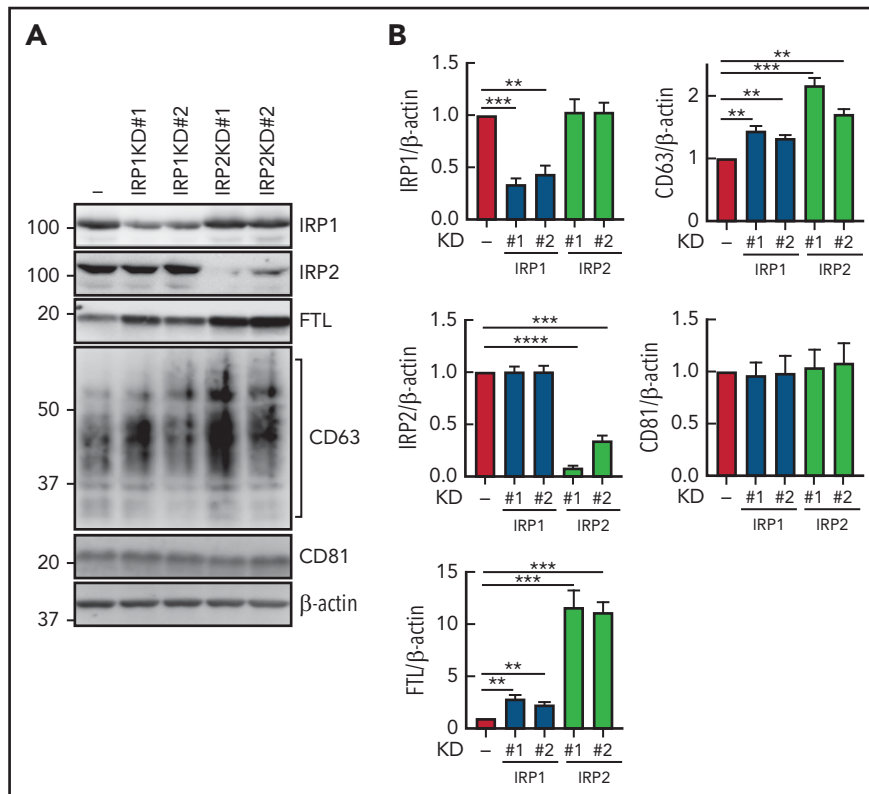


Figure 4. Silencing of IRP1 or IRP2 increases CD63 expression. (A) IRP1 and IRP2 expression were silenced by shRNA. Cells were lysed in lysis buffer, and 20 μg of protein per sample was analyzed with anti-IRP1, anti-IRP2, anti-CD63, anti-CD81, anti-FTL, and anti-β-actin antibodies. (B) Quantification of IRP1, IRP2, FTL, CD63, and CD81 from panel A. Results are mean ± SEM (3 experiments). Significance was determined using the Student t test. ***P* < .01; ****P* < .001; *****P* < .0001.

observed for THP1 cells, with iron loading markedly and significantly increasing the expression of CD63, FTH, and FTL, but not CD81, in cells and EVs (supplemental Figure 3A-E).

Under these conditions of iron loading, the cells were fully viable, as judged by their morphology and Trypan blue staining (>95%). As a control for generalized cell protein release into the medium as a result of cell death, we examined the expression of the intracellular proteins calnexin and protein disulphide isomerase (PDI; Figure 3C). These were robustly expressed in IMR90SV fibroblasts but were absent from their secreted EVs (Figure 3C).

To further assess EV secretion from cells upon iron loading, we used transmission electron microscopy of EVs from cellular supernatants, which revealed smaller EVs at 48 to 58 nm and larger EVs at 100 to 200 nm (Figure 3D-E). This examination also revealed a significant (*P* < .0001) increase in the number of EVs released upon cellular iron loading using FAC (Figure 3D-E). Collectively, the number of EVs secreted from cells upon iron loading with FAC was increased ~3 times (Figure 3D-E), and CD63 expression in secreted EVs was increased 3 to 4 times (Figure 3A). Thus, the number of CD63⁺ EVs secreted that contained FTH and FTL was increased by cellular iron loading.

Next, we determined whether ferritin in EVs contains iron because serum ferritin contains little iron.^{52,53} After loading IMR90SV fibroblasts with FAC (10 μg/mL) for 48 hours at

37°C compared with control medium, native polyacrylamide gel electrophoresis (PAGE) and immunoblotting confirmed the upregulation of FTH and FTL in cells and EVs (Figure 3F). Assessing whether these same samples contained iron-loaded ferritin, native PAGE was simultaneously performed and stained with Prussian blue to detect Fe⁺³. A single Prussian blue stained band was detected in both cells and EVs that migrated at the same level as ferritin and was evident only in FAC-treated samples (Figure 3F), indicating that cells and EVs contain Fe.

Examining the ratio of FTH or FTL protein between EVs and cells after FAC and comparing it with the control (Figure 3F; supplemental Figure 3A-D) demonstrated no alteration (Figure 3G; supplemental Figure 3E), indicating similar relative increases in FTH and/or FTL levels in cells and EVs upon iron loading. However, examining Figure 3F in which ferritin expression and iron levels were simultaneously assessed in cells and EVs under native conditions, a marked and significant (*P* < .0001) increase in FTH and FTL in EVs occurred after iron loading. Furthermore, there was an ~10-fold greater increase in FTH or FTL in cells compared with that in EVs after incubating cells with FAC (Figure 3F), whereas there was only 2 to 3 times more iron in intracellular ferritin compared with EV ferritin. Thus, when the iron:FTL or iron:FTH ratios were calculated, this demonstrated that a significantly (*P* < .05) greater proportion of ferritin in EVs is iron loaded compared with that in intracellular ferritin (Figure 3H).

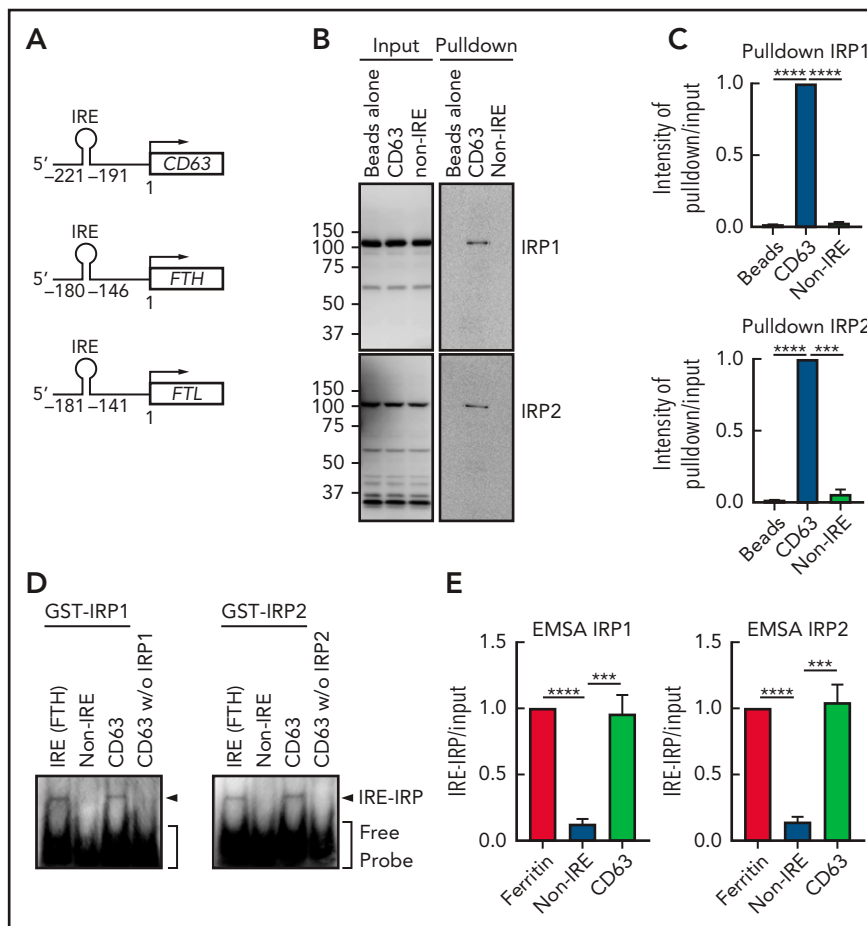


Figure 5. CD63 expression is posttranscriptionally regulated by the IRE-IRP system. (A) Schematic of the size and locations of the 5'-IRE domains in *CD63*, *FTH*, and *FTL* mRNAs. (B) *CD63* IRE-containing mRNA and non-IRE mRNA were biotinylated and mixed with a total protein extract from IMR90SV cells followed by pull-down using streptavidin beads. Input and pull-down proteins were analyzed by using anti-IRP1 and anti-IRP2 antibodies. Upon equal exposure of the input and pull-down, the percentage of IRP pulled down from the input was 2.5%. (C) Quantification of IRP1 and IRP2 intensity in panel B. (D) Purified GST-IRP1 or GST-IRP2 was mixed with biotinylated *FTH* IRE, *CD63* IRE, or non-IRE RNA (see "Methods" for details). Samples were loaded onto a native 6% TBE-polyacrylamide gel, transferred onto nylon membrane, and stained with streptavidin-horseradish peroxidase. (E) Quantification of shifted bands in panel D. Results are mean \pm SEM (3 experiments). Significance was determined by Student t test. *** $P < .001$; **** $P < .0001$.

The IRE-IRP system posttranscriptionally regulates CD63

Noting that *CD63* was upregulated by iron loading (Figures 2 and 3), we then aimed to dissect the mechanism involved. To examine the role of the IRE-IRP mechanism in regulating *CD63* by iron, we examined the presence of IREs in 5' and 3' UTR regions of *CD63* mRNA by using the IRE prediction software SIREs Web Server 2.0.³⁷ In the 5' UTR region of *CD63* mRNA, a 31-nucleotide long mRNA sequence was predicted as a consensus IRE (Figure 1A).^{32-34,37} The consensus features of typical (type I) IRE stem loops include (1) an apical pseudotri-loop of 6 nucleotides (CAG(U/A)GN; Figure 1A-B)³³⁻³⁵, (2) a midstem cytosine bulge (C8; Figure 1A-B), (3) a 5-bp upper helix (Figure 1A-B), and (4) a variable lower helix, and they are ~30 nucleotides in length.⁵⁴⁻⁵⁶

A number of IREs have been characterized in the 5' UTRs of mRNAs that are very similar to the consensus IRE observed in *CD63* mRNA (Figure 1A).^{32,57-61} Functional IREs that bind IRPs are also found in the 3' UTR (Figure 1B).⁶²⁻⁶⁶ The stability of the IRP1-IRE mRNA complex is dictated by the free energy change

(Figure 1A-B; Table 1),⁶⁷ with the *CD63* IRE (-2.3 kcal/mol) being within the range of consensus type I IREs (ie, -1.3 to -10.6 kcal/mol; Figure 1A-B), whereas atypical type II IREs demonstrate very minimal stability (Figure 1A).³⁷

The human *CD63* IRE was conserved in the 5' UTR in 4 of 25 primates assessed (Table 1). Sixty organisms were also examined for IREs in the 5' UTR using SIREs,³⁷ with the identification of high and medium stringency systematic evolution of ligands by exponential enrichment motif (SELEX) IRE motifs in the 5' UTR of *CD63* in 9 mammals (Table 1). This level of stringency captures classical IREs.³⁷

To examine the role of IRPs in *CD63* regulation, studies began by using lentiviral short hairpin RNAs (shRNAs) against *IRP1* and *IRP2* in IMR90SV fibroblasts (Figure 4A-B). Two *IRP1* shRNAs (#1 and #2) led to a significant ($P < .001$ to $P < .01$) 60% and 50% downregulation of *IRP1* in *IRP1KD#1* and *IRP1KD#2* cells, respectively, but had no significant effect on *IRP2* (Figure 4A-B). The decreased *IRP1* in *IRP1KD#1* and *IRP1KD#2* resulted in a slight, but significant ($P < .01$) twofold to threefold increase in

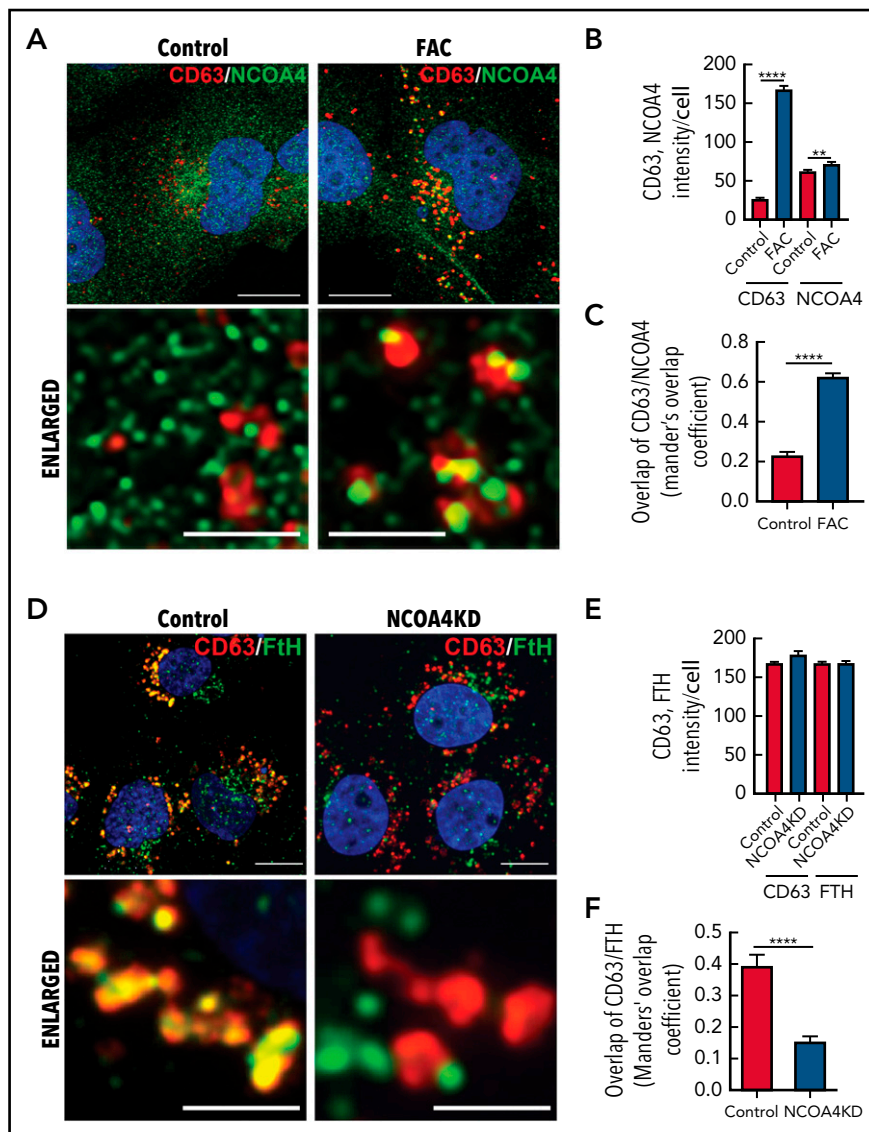


Figure 6. Iron repletion leads to the colocalization of CD63 and NCOA4 into the same vesicle. (A) IMR90SV cells were incubated in medium (–FBS) (control) or medium supplemented with FAC (10 $\mu\text{g}/\text{mL}$) for 16 hours at 37°C. Cells were fixed and stained with anti-NCOA4 (green) and anti-CD63 (red) antibodies. (B) Quantification of CD63 and NCOA4 intensity in panel A. (C) Quantification of CD63 and NCOA4 colocalization indicated by Manders' overlap coefficient. (D) Control and NCOA4KD IMR90SV cells were incubated for 16 hours at 37°C with 10 $\mu\text{g}/\text{mL}$ FAC. Cells were fixed and stained with anti-FTH (green) and anti-CD63 (red) antibodies. (E) Quantification of CD63 and FTH intensity in panel D. (F) Quantification of CD63 and FTH colocalization by Manders' overlap coefficient. (A,D) Thin scale bar, 10 μm ; thick scale bar, 2.5 μm . For analysis, >60 cells were examined per condition over 3 experiments. Results are mean \pm SEM (3 experiments). Significance was determined using the Student t test. ** $P < .01$; **** $P < .0001$.

FTL compared with the respective control. Examining CD63, a slight but significant ($P < .01$) increase was observed in IRP1KD#1 and IRP1KD#2 cells (Figure 4A-B). In contrast, no significant alteration in CD81 was found for IRP1KD#1 and IRP1KD#2 cells.

The 2 IRP2 shRNAs #1 and #2 led to a significant ($P < .001$ to $P < .01$) 90% and 70% decrease of IRP2 in IRP2KD#1 and IRP1KD#2 cells, respectively, but had no significant effect on IRP1 (Figure 4A-B). The downregulation of IRP2 caused a significant ($P < .01$ to $P < .001$) increase in FTL and CD63 (Figure 4A-B), whereas there was no effect on CD81. To summarize, the IRP1 and IRP2 shRNAs #1 and #2 demonstrate that decreased IRP1 or IRP2 leads to posttranscriptional de-repression and upregulation of the IRE-containing targets FTL and CD63.

The IRE domain in human CD63 mRNA is located at –221 to –191 bp upstream of the first methionine, which is similar to the IRE of FTH (–180 to –146 bp)³² or FTL (–181 to –141 bp)⁶¹ (Figure 5A). We then assessed whether the consensus IRE in CD63 mRNA could function as an IRP-binding motif by using RNA pulldown (Figure 5B-C) and native EMSAs (Figure 5D-E). The 31-bp IRE in the CD63 5' UTR was biotinylated, mixed with IMR90SV cell extracts, and pulled down using biotin-streptavidin beads. The CD63 IRE sequence led to a significant ($P < .0001$ to $P < .001$) increase in IRP1 and IRP2 binding compared with the beads alone or the non-IRE control (Figure 5B-C).

Next, EMSA was performed using purified human recombinant GST-IRP1 and GST-IRP2 (Figure 5D). Upon mixing FTH-IRE (positive control) or CD63 5' UTR RNA with GST-IRP1 or GST-IRP2, a

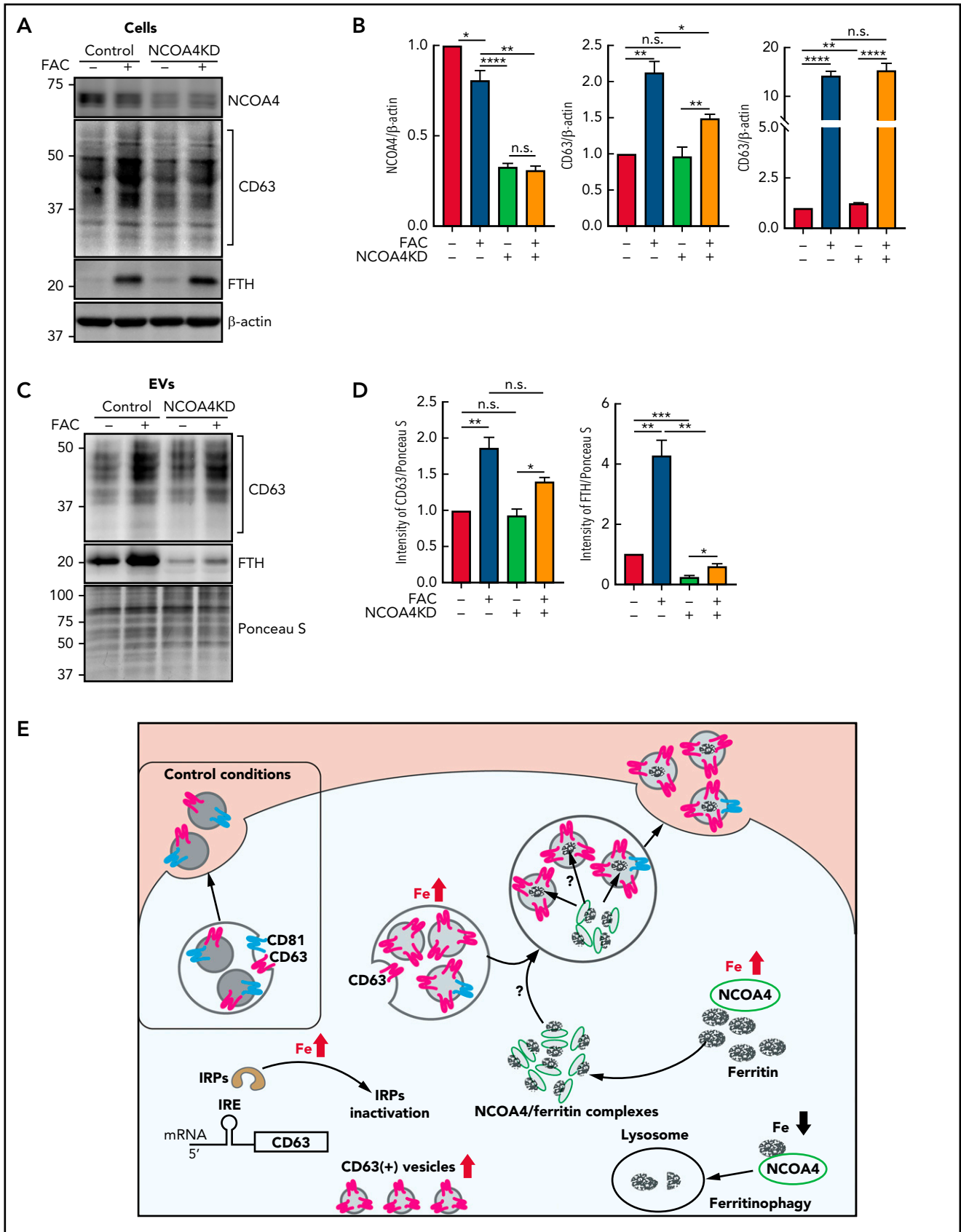


Figure 7. Ferritin secretion through EVs is dependent on NCOA4 expression. (A) IMR90SV cells were incubated in the presence or absence of FAC (10 μ g/mL) for 48 hours at 37°C. Isolated EVs from cell culture supernatants were collected by the procedures described in “Methods.” (A) Total cell lysates (20 μ g of protein per sample) and (C) EVs (20 μ g of protein per sample) were analyzed by immunoblotting with anti-CD63, anti-FTH, anti-NCOA4, and anti- β -actin antibodies. (B) Quantification

single shifted band became apparent, which demonstrated the functional interaction of the IRE with IRP1 or IRP2 (Figure 5D-E). Notably, the non-IRE containing control probe used in Figure 5B and the CD63 IRE added without IRP1 or IRP2 were negative. These results demonstrate that the consensus IRE in *CD63* mRNA is functional in terms of IRP1 and IRP2 binding, suggesting that CD63 could be regulated via this mechanism.

NCOA4 associates with CD63⁺ EVs and transfers ferritin into EVs

NCOA4 acts as a receptor that delivers iron-laden ferritin to lysosomes for iron release during iron depletion.⁶⁸ We hypothesized that NCOA4 may also act as a ferritin trafficking receptor, which can fuse with CD63⁺ EVs and transfer ferritin to the secretory pathway. To confirm this, IMR90SV cells were incubated with medium (-FBS) (control) or medium containing 10 µg/mL FAC for 16 hours at 37°C, and then we examined the cells using confocal immunofluorescence microscopy (Figure 6A-C).

Under control conditions, NCOA4 (green) appeared in the cytosol as small, perinuclear, vesicle-like structures (Figure 6A, left), in agreement with studies indicating that NCOA4 localizes to the Golgi apparatus⁶⁹ and/or microtubules.⁷⁰ However, upon iron repletion with FAC, CD63 (red) significantly ($P < .0001$) increased compared with the control (Figure 6A-B). Under these conditions, NCOA4 became associated with larger CD63⁺ vesicles (Figure 6A, right) that resulted in a significant ($P < .0001$) increase in NCOA4 and CD63 colocalization upon iron repletion with FAC (Figure 6C). A previous study demonstrated that NCOA4 was degraded after iron loading through a ubiquitin-proteasome pathway.⁶⁸ We determined, by using IMR90SV fibroblasts, that total NCOA4 expression was not altered upon incubation with FAC (2 to 24 hours; supplemental Figure 4Ai). However, during this time course, the number of NCOA4 foci per cell decreased significantly, and the average size of NCOA4 foci concurrently increased significantly, suggesting that foci were coalescing (supplemental Figure 4Aii). Moreover, by examining iron loading over 2 to 24 hours, expression of NCOA4 and its ubiquitin ligase HECT and RLD domain-containing E3 ubiquitin protein ligase 2 (HERC2) did not change significantly, whereas IRP2, FTL, and FTH were markedly altered after only 6 hours (supplemental Figure 4D-E). Collectively, these data (Figure 6A; supplemental Figure 4) demonstrate that upon iron loading, NCOA4 puncta coalesce into larger structures and colocalize with CD63⁺ vesicles, possibly to facilitate ferritin trafficking into EVs.

Given these latter results, we explored whether ferritin is transferred to CD63⁺ vesicles via NCOA4. NCOA4 was silenced in IMR90SV cells to generate NCOA4KD cells and was compared with scramble control cells (Figure 6D-F). These cells were incubated for 16 hours at 37°C with 10 µg/mL FAC (-FBS), and FTH and CD63 were investigated by using confocal microscopy. There was no change in CD63 or FTH intensity in NCOA4KD

cells compared with scramble control cells (Figure 6E). However, upon examination, scramble control cells, CD63 (red), and FTH (green) containing vesicular structures strongly merge, leading to yellow fluorescence (Figure 6D), suggesting association of CD63 with FTH. Importantly, there was a significant ($P < .0001$) decrease in colocalization of FTH with CD63⁺ vesicles in NCOA4KD cells compared with the scrambled control (Figure 6F). In fact, in NCOA4KD cells, FTH was observed in vesicle-like structures that no longer merge with CD63-containing vesicles (Figure 6D). This latter finding indicated that loss of NCOA4 prevented association of FTH with CD63-containing vesicles. In summary, Figure 6 shows that under iron loading, NCOA4 associates with CD63⁺ EVs and transfers ferritin into these structures.

FTH secretion through EVs under iron loading is dependent on NCOA4 expression

The results in Figure 6A-C demonstrate association of NCOA4 and CD63-containing vesicles under iron loading, so we performed additional studies to determine whether FTH secretion through EVs was dependent on NCOA4 expression (Figure 7A-D). This was assessed by implementing NCOA4KD cells compared with the respective scramble control cells after incubation with or without 10 µg/mL FAC for 48 hours at 37°C in the presence of 0.5% FBS that had been depleted of bovine EVs.⁵¹ Cells were incubated for 48 hours to ensure secretion of sufficient EVs. Incubation of scramble control cells with FAC caused a slight ($P < .05$) decrease of NCOA4 (Figure 7A-B). By examining NCOA4KD cells, we determined that NCOA4 was downregulated to 30% of the scramble control in the presence or absence of FAC (Figure 7A-B). Iron loading significantly ($P < .01$ to $P < .05$) increased CD63 or FTH irrespective of the decreased NCOA4 in NCOA4KD cells (Figure 7A-B). Silencing of NCOA4 slightly increased FTH in NCOA4KD cells in the absence of FAC, which is consistent with its catabolic role in ferritinophagy⁶³ and the loss of function after silencing.

Examination of secreted EVs showed that CD63 was significantly ($P < .01$ to $P < .05$) increased in EVs after incubation of cells with FAC in scramble control cells and NCOA4KD cells (Figure 7C-D). FTH was significantly ($P < .01$) increased by FAC in the scramble control cells compared with control medium. Notably, FTH was significantly ($P < .001$ to $P < .01$) higher in the presence and absence of FAC in the scramble control cells compared with their respective treatments in NCOA4KD cells (Figure 7C-D). These results indicate that NCOA4 silencing markedly decreased FTH in isolated EVs and also indicate that NCOA4 plays a role in ferritin secretion via EVs through CD63⁺ vesicles.

Discussion

This study has identified the IRE-IRP-dependent posttranscriptional regulation of CD63, one of the major EV-associated proteins involved in exosome secretion.⁶ Furthermore, CD63⁺ EVs associate with NCOA4 ferritin vesicles within cells, with NCOA4 transferring ferritin to these structures, which are then secreted

Figure 7 (continued) of NCOA4, CD63, and FTH in panel A. (D) Quantification of CD63 and FTH in panel C. Results are mean \pm SEM (3 experiments). (E) Schematic illustrating the mechanism of ferritin iron secretion that occurs by EVs upon iron repletion. Iron repletion induces IRP inactivation, which initiates both ferritin and CD63 translation via the dissociation of IRP from the canonical type I IRE in the 5' UTR of *CD63* mRNA. Upon iron repletion, CD63 expression, but not CD81 expression, in EVs is markedly increased, and CD63 is important for ferritin-mediated iron secretion from cells. The ferritin cargo receptor NCOA4 closely associates with CD63⁺ vesicles under iron loading and is necessary for the association of ferritin and CD63 and also ferritin secretion in EVs. It will be necessary to investigate the mechanism of how ferritin is transferred from NCOA4-ferritin complexes⁶⁸ to EVs. In contrast to iron loading, upon iron depletion, ferritin is degraded in lysosomes via the autophagic pathway of ferritinophagy.⁶⁸ Significance was determined by the Student t test. * $P < .05$; ** $P < .01$; *** $P < .001$; **** $P < .0001$.

under conditions of cellular iron loading (Figure 7E). The iron-regulated secretion of the major iron storage protein ferritin via CD63 poses significant consequences for understanding regulation of cellular iron metabolism, particularly local cell-to-cell exchange of ferritin.

Ferritin secretion occurs in many normal and neoplastic cell types,¹³⁻²⁷ with iron-rich ferritin being secreted via the multivesicular body-exosome pathway¹² and FTH being demonstrated in exosomes.^{11,12} EVs are important for intercellular communication, with ferritin secreted from macrophages being an additional iron source for erythroid cells.²¹

Of note, NCOA4 functions as an intracellular ferritin cargo receptor and directly binds FTH, with ferritin being incorporated into autophagosomes to initiate ferritinophagy under iron deprivation (catabolic) conditions.⁶⁸ In contrast, under iron loading (anabolic) conditions in which CD63 is upregulated, the ferritin cargo receptor NCOA4 closely associates with CD63⁺ vesicles (Figure 6A). Furthermore, ferritin was identified within CD63⁺ EVs, and cells depleted of NCOA4 resulted in impaired ferritin secretion in EVs. In fact, examining NCOA4-depleted cells showed that ferritin was observed outside CD63⁺ vesicles (Figure 6D), which is consistent with a previous report demonstrating that aggregation of insoluble ferritin in the cytoplasm was enhanced under NCOA4-depleted conditions.^{70,71} Collectively, ferritin follows 2 distinct pathways via NCOA4 that are dependent on the metabolic state: (1) lysosomal degradation of ferritin during iron deficiency that mobilizes stored iron⁶⁸ and (2) extracellular secretion of ferritin through CD63⁺ EVs under anabolic conditions when cells are iron loaded.

The ability of the cells to regulate cellular iron mobilization via ferritin released through EVs adds another dimension to the mechanisms of cellular iron efflux that includes iron release mediated by ferroportin, which is regulated by the IRE-IRP system⁶⁰ and hepcidin.⁷² Having 2 well-regulated systems of iron mobilization (secretory ferritin and iron released from ferroportin that is then bound by transferrin) could be critical for fine-tuning cellular iron demands. Previous studies have indicated that serum ferritin is iron poor.^{52,53} Our results demonstrate that only after cellular iron loading did secreted EVs contain iron-loaded ferritin (Figure 3F,H). Thus, cellular iron status seems to be critical in terms of the iron loading of secreted ferritin in EVs and is important for considering local cellular ferritin and iron metabolism.

In summary, CD63, which is involved in EV secretion,⁶ is regulated by the IRE-IRP system, with a canonical IRE in the 5' UTR of CD63 mRNA regulating its expression. Iron loading resulted in secretion of CD63⁺ EVs from cells that contained iron-loaded ferritin (Figure 3A-B), and intracellular ferritin was shown to be transferred via NCOA4 to CD63⁺

EVs that are secreted (Figure 7E). Such a mechanism provides new understanding regarding the regulation of iron metabolism, especially local cell-to-cell exchange of ferritin and iron.

Acknowledgments

This work was supported by Japan Society for the Promotion of Science (JSPS) Grants-in-Aid for Scientific Research (KAKENHI) (19K23722 and 20K07309) (I.Y.); grants from the National Health and Medical Research Council of Australia (APP1144456 and APP1144829) and a Senior Principal Research Fellowship (APP1159596); a grant from the Australian Research Council (DP200103530) (D.R.R.); and grants from the Japan Science and Technology Agency (JST) Core Research for Evolutional Science and Technology (CREST) (JPMJCR19H4) and JSPS KAKENHI (JP20H05502) (S.T.).

Electron microscopic analyses were supported by Koji Itakura, Division of Medical Research Engineering, Nagoya University Graduate School of Medicine.

Authorship

Contribution: I.Y. designed all of experiments and performed the research; H.S.D. co-designed some experiments and analyzed the data; I.Y., H.S.D., and D.R.R. analyzed the data and wrote and edited the manuscript; S.T. reviewed and edited the manuscript; and F.K. supervised I.Y., provided academic guidance, and supported the research project.

Conflict-of-interest disclosure: The authors declare no competing financial interests.

ORCID profiles: I.Y., 0000-0002-1945-5473; D.R.R., 0000-0003-0960-6415; H.S.D., 0000-0002-2240-1230; S.T., 0000-0002-5757-1109; K.F., 0000-0002-0949-5914.

Correspondence: Des R. Richardson, Centre for Cancer Cell Biology and Drug Discovery, Griffith Institute for Drug Discovery, Griffith University, Nathan, Brisbane, QLD 4212, Australia; e-mail: d.richardson@griffith.edu.au; and Shinya Toyokuni, Department of Pathology and Biological Responses, Nagoya University Graduate School of Medicine, Nagoya 466-8550, Japan; e-mail: toyokuni@med.nagoya-u.ac.jp.

Footnotes

Submitted 1 February 2021; accepted 24 June 2021; prepublished online on *Blood* First Edition 15 July 2021. DOI 10.1182/blood.2021010995.

*D.R.R. and S.T. contributed equally to this work as senior corresponding authors.

The online version of this article contains a data supplement.

There is a *Blood* Commentary on this article in this issue.

The publication costs of this article were defrayed in part by page charge payment. Therefore, and solely to indicate this fact, this article is hereby marked "advertisement" in accordance with 18 USC section 1734.

REFERENCES

1. Yáñez-Mó M, Siljander PR-M, Andreu Z, et al. Biological properties of extracellular vesicles and their physiological functions. *J Extracell Vesicles*. 2015;4(1):27066.
2. Gandham S, Su X, Wood J, et al. Technologies and standardization in research on extracellular vesicles. *Trends Biotechnol*. 2020;38(10):1066-1098.
3. Andreu Z, Yáñez-Mó M. Tetraspanins in extracellular vesicle formation and function. *Front Immunol*. 2014;5:442.
4. Pols MS, Klumperman J. Trafficking and function of the tetraspanin CD63. *Exp Cell Res*. 2009;315(9):1584-1592.
5. Kobayashi T, Vischer UM, Rosnoble C, et al. The tetraspanin CD63/lamp3 cycles between endocytic and secretory compartments in human endothelial cells. *Mol Biol Cell*. 2000;11(5):1829-1843.
6. Hurwitz SN, Conlon MM, Rider MA, Brownstein NC, Meckes DG Jr. Nanoparticle analysis sheds budding

- insights into genetic drivers of extracellular vesicle biogenesis. *J Extracell Vesicles*. 2016;5(1):31295.
7. Israels SJ, McMillan-Ward EM. CD63 modulates spreading and tyrosine phosphorylation of platelets on immobilized fibrinogen. *Thromb Haemost*. 2005;93(2):311-318.
 8. Dogrammatzis C, Deschamps T, Kalamvoki M. Biogenesis of extracellular vesicles during Herpes Simplex Virus 1 infection: role of the CD63 tetraspanin. *J Virol*. 2019;93(2):e01850-18.
 9. Lawson DM, Artymiuk PJ, Yewdall SJ, et al. Solving the structure of human H ferritin by genetically engineering intermolecular crystal contacts. *Nature*. 1991;349(6309):541-544.
 10. Ponka P, Beaumont C, Richardson DR. Function and regulation of transferrin and ferritin. *Semin Hematol*. 1998;35(1):35-54.
 11. Mrowczynski OD, Madhankumar AB, Slagle-Webb B, Lee SY, Zacharia BE, Connor JR. HFE genotype affects exosome phenotype in cancer. *Biochim Biophys Acta Gen Subj*. 2017;1861(8):1921-1928.
 12. Truman-Rosentsvit M, Berenbaum D, Spektor L, et al. Ferritin is secreted via 2 distinct nonclassical vesicular pathways. *Blood*. 2018;131(3):342-352.
 13. Lescoat G, Hubert N, Moirand R, Jego P, Pasdeloup N, Brissot P. Iron load increases ferritin synthesis and secretion in adult human hepatocyte cultures. *Liver*. 1991;11(1):24-29.
 14. Goto Y, Paterson M, Listowsky I. Iron uptake and regulation of ferritin synthesis by hepatoma cells in hormone-supplemented serum-free media. *J Biol Chem*. 1983;258(8):5248-5255.
 15. Ghosh S, Hevi S, Chuck SL. Regulated secretion of glycosylated human ferritin from hepatocytes. *Blood*. 2004;103(6):2369-2376.
 16. Tran TN, Eubanks SK, Schaffer KJ, Zhou CY, Linder MC. Secretion of ferritin by rat hepatoma cells and its regulation by inflammatory cytokines and iron. *Blood*. 1997;90(12):4979-4986.
 17. Kidane TZ, Sauble E, Linder MC. Release of iron from ferritin requires lysosomal activity. *Am J Physiol Cell Physiol*. 2006;291(3):C445-C455.
 18. Beaumont C, Dugast I, Renaudie F, Souroujon M, Grandchamp B. Transcriptional regulation of ferritin H and L subunits in adult erythroid and liver cells from the mouse. Unambiguous identification of mouse ferritin subunits and in vitro formation of the ferritin shells. *J Biol Chem*. 1989;264(13):7498-7504.
 19. Cohen LA, Gutierrez L, Weiss A, et al. Serum ferritin is derived primarily from macrophages through a nonclassical secretory pathway. *Blood*. 2010;116(9):1574-1584.
 20. Yuan X-M, Li W, Baird SK, Carlsson M, Meleforts O. Secretion of ferritin by iron-laden macrophages and influence of lipoproteins. *Free Radic Res*. 2004;38(10):1133-1142.
 21. Leimberg MJ, Prus E, Konijn AM, Fibach E. Macrophages function as a ferritin iron source for cultured human erythroid precursors. *J Cell Biochem*. 2008;103(4):1211-1218.
 22. Connor JR, Zhang X, Nixon AM, Webb B, Perno JR. Comparative evaluation of nephrotoxicity and management by macrophages of intravenous pharmaceutical iron formulations. *PLoS One*. 2015;10(5):e0125272.
 23. Cosme J, Guo H, Hadipour-Lakmehsari S, Emili A, Gramolini AO. Hypoxia-induced changes in the fibroblast secretome, exosome, and whole-cell proteome using cultured, cardiac-derived cells isolated from neonatal mice. *J Proteome Res*. 2017;16(8):2836-2847.
 24. Hann HW, Stahlhut MW, Evans AE. Source of increased ferritin in neuroblastoma: studies with concanavalin A-sepharose binding. *J Natl Cancer Inst*. 1986;76(6):1031-1033.
 25. Selig RA, Madafiglio J, Haber M, Norris MD, White L, Stewart BW. Ferritin production and desferrioxamine cytotoxicity in human neuroblastoma cell lines. *Anticancer Res*. 1993;13(3):721-725.
 26. Mukherjee C, Kling T, Russo B, et al. Oligodendrocytes provide antioxidant defense function for neurons by secreting ferritin heavy chain. *Cell Metab*. 2020;32(2):259-272.e10.
 27. Greco TM, Seeholzer SH, Mak A, Spruce L, Ischiropoulos H. Quantitative mass spectrometry-based proteomics reveals the dynamic range of primary mouse astrocyte protein secretion. *J Proteome Res*. 2010;9(5):2764-2774.
 28. Wang W, Knovich MA, Coffman LG, Torti FM, Torti SV. Serum ferritin: Past, present and future. *Biochim Biophys Acta*. 2010;1800(8):760-769.
 29. Leibold EA, Laudano A, Yu Y. Structural requirements of iron-responsive elements for binding of the protein involved in both transferrin receptor and ferritin mRNA post-transcriptional regulation. *Nucleic Acids Res*. 1990;18(7):1819-1824.
 30. Richardson DR, Ponka P. The molecular mechanisms of the metabolism and transport of iron in normal and neoplastic cells. *Biochim Biophys Acta*. 1997;1331(1):1-40.
 31. Yanatori I, Richardson DR, Toyokuni S, Kishi F. The new role of poly (rC)-binding proteins as iron transport chaperones: Proteins that could couple with inter-organelle interactions to safely traffic iron. *Biochim Biophys Acta Gen Subj*. 2020;1864(11):129685.
 32. Eisenstein RS, Blemings KP. Iron regulatory proteins, iron responsive elements and iron homeostasis. *J Nutr*. 1998;128(12):2295-2298.
 33. Henderson BR, Menotti E, Bonnard C, Kühn LC. Optimal sequence and structure of iron-responsive elements. Selection of RNA stem-loops with high affinity for iron regulatory factor. *J Biol Chem*. 1994;269(26):17481-17489.
 34. Henderson BR, Menotti E, Kühn LC. Iron regulatory proteins 1 and 2 bind distinct sets of RNA target sequences. *J Biol Chem*. 1996;271(9):4900-4908.
 35. Butt J, Kim HY, Basilion JP, et al. Differences in the RNA binding sites of iron regulatory proteins and potential target diversity. *Proc Natl Acad Sci U S A*. 1996;93(9):4345-4349.
 36. Rider MA, Hurwitz SN, Meckes DG Jr. ExtraPEG: A polyethylene glycol-based method for enrichment of extracellular vesicles. *Sci Rep*. 2016;6(1):23978.
 37. Campillos M, Cases I, Hentze MW, Sanchez M. SIREs: searching for iron-responsive elements. *Nucleic Acids Res*. 2010;38(Web Server issue):W360-W367.
 38. Hurwitz SN, Cheerathodi MR, Nkosi D, York SB, Meckes DG Jr. Tetraspanin CD63 bridges autophagic and endosomal processes to regulate exosomal secretion and intracellular signaling of Epstein-Barr virus LMP1. *J Virol*. 2018;92(5):e01969-17.
 39. Bae D-H, Lane DJR, Siafakas AR, et al. Acireductone dioxygenase 1 (ADI1) is regulated by cellular iron by a mechanism involving the iron chaperone, PCBP1, with PCBP2 acting as a potential co-chaperone. *Biochim Biophys Acta Mol Basis Dis*. 2020;1866(10):165844.
 40. Tominaga N, Hagiwara K, Kosaka N, Honma K, Nakagama H, Ochiya T. RPN2-mediated glycosylation of tetraspanin CD63 regulates breast cancer cell malignancy. *Mol Cancer*. 2014;13(1):134.
 41. Ageberg M, Lindmark A. Characterisation of the biosynthesis and processing of the neutrophil granule membrane protein CD63 in myeloid cells. *Clin Lab Haematol*. 2003;25(5):297-306.
 42. Shull GE, Theil EC. Translational control of ferritin synthesis by iron in embryonic reticulocytes of the bullfrog. *J Biol Chem*. 1982;257(23):14187-14191.
 43. Theil EC. Regulation of ferritin and transferrin receptor mRNAs. *J Biol Chem*. 1990;265(9):4771-4774.
 44. Lui GYL, Obeidy P, Ford SJ, et al. The iron chelator, deferasirox, as a novel strategy for cancer treatment: oral activity against human lung tumor xenografts and molecular mechanism of action. *Mol Pharmacol*. 2013;83(1):179-190.
 45. Ford SJ, Obeidy P, Lovejoy DB, et al. Deferasirox (ICL670A) effectively inhibits oesophageal cancer growth in vitro and in vivo. *Br J Pharmacol*. 2013;168(6):1316-1328.
 46. Edgar JR, Manna PT, Nishimura S, Banting G, Robinson MS. Tetherin is an exosomal tether. *eLife*. 2016;5:e17180.
 47. Klionsky DJ, Abdel-Aziz AK, Abdelfatah S, et al. Guidelines for the use and interpretation of assays for monitoring autophagy (4th edition). *Autophagy*. 2021;17(1):1-382.

48. Yamamoto A, Tagawa Y, Yoshimori T, Moriyama Y, Masaki R, Tashiro Y. Bafilomycin A1 prevents maturation of autophagic vacuoles by inhibiting fusion between autophagosomes and lysosomes in rat hepatoma cell line, H-4-II-E cells. *Cell Struct Funct.* 1998;23(1):33-42.
49. Kondo Y, Kanzawa T, Sawaya R, Kondo S. The role of autophagy in cancer development and response to therapy. *Nat Rev Cancer.* 2005;5(9):726-734.
50. Lum JJ, DeBerardinis RJ, Thompson CB. Autophagy in metazoans: cell survival in the land of plenty. *Nat Rev Mol Cell Biol.* 2005; 6(6):439-448.
51. Heath N, Grant L, De Oliveira TM, et al. Rapid isolation and enrichment of extracellular vesicle preparations using anion exchange chromatography. *Sci Rep.* 2018; 8(1):5730.
52. Worwood M, Dawkins S, Wagstaff M, Jacobs A. The purification and properties of ferritin from human serum. *Biochem J.* 1976;157(1): 97-103.
53. Arosio P, Yokota M, Drysdale JW. Characterization of serum ferritin in iron overload: possible identity to natural apoferritin. *Br J Haematol.* 1977;36(2):199-207.
54. Selezneva AI, Walden WE, Volz KW. Nucleotide-specific recognition of iron-responsive elements by iron regulatory protein 1. *J Mol Biol.* 2013;425(18):3301-3310.
55. Sierzputowska-Gracz H, McKenzie RA, Theil EC. The importance of a single G in the hairpin loop of the iron responsive element (IRE) in ferritin mRNA for structure: an NMR spectroscopy study. *Nucleic Acids Res.* 1995;23(1):146-153.
56. Walden WE, Selezneva A, Volz K. Accommodating variety in iron-responsive elements: Crystal structure of transferrin receptor 1 B IRE bound to iron regulatory protein 1. *FEBS Lett.* 2012;586(1):32-35.
57. Cox TC, Bawden MJ, Martin A, May BK. Human erythroid 5-aminolevulinic synthase: promoter analysis and identification of an iron-responsive element in the mRNA. *EMBO J.* 1991;10(7):1891-1902.
58. Sanchez M, Galy B, Muckenthaler MU, Hentze MW. Iron-regulatory proteins limit hypoxia-inducible factor-2alpha expression in iron deficiency. *Nat Struct Mol Biol.* 2007; 14(5):420-426.
59. Schalinske KL, Chen OS, Eisenstein RS. Iron differentially stimulates translation of mitochondrial aconitase and ferritin mRNAs in mammalian cells. Implications for iron regulatory proteins as regulators of mitochondrial citrate utilization. *J Biol Chem.* 1998;273(6):3740-3746.
60. Donovan A, Brownlie A, Zhou Y, et al. Positional cloning of zebrafish ferroportin1 identifies a conserved vertebrate iron exporter. *Nature.* 2000;403(6771):776-781.
61. Missirlis F, Kosmidis S, Brody T, et al. Homeostatic mechanisms for iron storage revealed by genetic manipulations and live imaging of Drosophila ferritin. *Genetics.* 2007;177(1):89-100.
62. Frazer DM, Wilkins SJ, Becker EM, et al. A rapid decrease in the expression of DMT1 and Dcytb but not Ireg1 or hephaestin explains the mucosal block phenomenon of iron absorption. *Gut.* 2003;52(3):340-346.
63. Yanatori I, Kishi F. DMT1 and iron transport. *Free Radic Biol Med.* 2019;133:55-63.
64. Müllner EW, Kühn LC. A stem-loop in the 3' untranslated region mediates iron-dependent regulation of transferrin receptor mRNA stability in the cytoplasm. *Cell.* 1988; 53(5):815-825.
65. Sanchez M, Galy B, Dandekar T, et al. Iron regulation and the cell cycle: identification of an iron-responsive element in the 3'-untranslated region of human cell division cycle 14A mRNA by a refined microarray-based screening strategy. *J Biol Chem.* 2006;281(32):22865-22874.
66. Cmejla R, Petrak J, Cmejlova J. A novel iron responsive element in the 3'UTR of human MRCKalpha. *Biochem Biophys Res Commun.* 2006;341(1):158-166.
67. Khan MA, Walden WE, Theil EC, Goss DJ. Thermodynamic and kinetic analyses of iron response element (IRE)-mRNA binding to iron regulatory protein, IRP1. *Sci Rep.* 2017; 7(1):8532.
68. Mancias JD, Wang X, Gygi SP, Harper JW, Kimmelman AC. Quantitative proteomics identifies NCOA4 as the cargo receptor mediating ferritinophagy. *Nature.* 2014; 509(7498):105-109.
69. Hara Y, Yanatori I, Tanaka A, et al. Iron loss triggers mitophagy through induction of mitochondrial ferritin. *EMBO Rep.* 2020; 21(11):e50202.
70. Dowdle WE, Nyfeler B, Nagel J, et al. Selective VPS34 inhibitor blocks autophagy and uncovers a role for NCOA4 in ferritin degradation and iron homeostasis in vivo. *Nat Cell Biol.* 2014;16(11):1069-1079.
71. Bellelli R, Federico G, Matte' A, et al. NCOA4 deficiency impairs systemic iron homeostasis. *Cell Rep.* 2016;14(3):411-421.
72. Nemeth E, Tuttle MS, Powelson J, et al. Hepcidin regulates cellular iron efflux by binding to ferroportin and inducing its internalization. *Science.* 2004;306(5704): 2090-2093.